Microchimica Acta (2020) 187:275
https://doi.org/10.1007/s00604-020-04233-7

ORIGINAL PAPER

Electrochemical biosensor for the epithelial cancer biomarker EpCAM based on reduced graphene oxide modified with nanostructured titanium dioxide

Owais Jalil[1] · Chandra Mouli Pandey[1] · Devendra Kumar[1]

Received: 30 August 2019 / Accepted: 23 March 2020
© Springer-Verlag GmbH Austria, part of Springer Nature 2020

Abstract

An electrochemical immunosensor has been fabricated for the early determination of epithelial cell adhesion molecules (EpCAM, tumor biomarker) antigen using reduced graphene oxide (rGO) modified with nanostructured titanium dioxide (TiO_2). The hydrothermally synthesized rGO@TiO_2 nanocomposite has been electrophoretically deposited on indium tin oxide (ITO) coated glass substrate, and the deposition was confirmed using various spectroscopic, microscopic, and electrochemical techniques. The fabricated rGO@TiO_2/ITO electrode shows improved electron transfer kinetics with an electron transfer rate constant of 1.93×10^{-7} cm·s^{-1}. Furthermore, the rGO@TiO_2/ITO electrodes were used for the covalent immobilization of monoclonal EpCAM antibodies. Electrochemical determination of the EpCAM cancer biomarker is achieved using differential pulse voltammetry by scanning the potential from − 0.4 to 0.8 V with an amplitude of 50 mV. The rGO@TiO_2-based biosensor shows high sensitivity (3.24 μA·mL·ng^{-1}·cm^{-2}), wide detection range (0.01 ng·mL^{-1} to 60 ng·mL^{-1}), and low detection limit (0.0065 ng·mL^{-1}, S/N = 3). The fabricated biosensor is highly stable and regenerable and has been successfully applied to the determination of EpCAM in spiked human serum samples.

Keywords Biomarker · Cancer · Epithelial cell adhesion molecules · Electrophoretic deposition · Electrochemical biosensor · Graphene oxide · Titanium dioxide

Introduction

The early detection and quantification of cancer biomarkers provide an efficient pathway to observe tumor progression and relate them to specific cancer types. In this context, epithelial cell adhesion molecules (EpCAM) have been considered a prognostic tumor biomarker for cancer diagnosis [1–3]. EpCAM is a glycosylated transmembrane protein, which is expressed on the surface of circulating tumor cells, and the overexpression of EpCAM has generally been found in the carcinomas of the breast, stomach, colon, rectum, prostate, biliary tract, pancreas, etc. [4, 5]. For the detection of EpCAM, techniques such as cytometry, enzyme-linked immunosorbent assays, and polymerase chain reaction have been widely used [6, 7]. However, these methods are usually expensive, complicated, time-consuming, and even require highly skilled human resources [8]. Therefore, there is an urgency for the development of an effective alternative method for early, sensitive, affordable, and reliable determination of EpCAM.

Some immunosensor based on electrochemical [9], fluorescence [10, 11], surface plasmon resonance [12], and colorimetric techniques have been reported for the detection of EpCAM. Shiddiky et al. have successfully functionalized 2D graphene oxide (GO) nanosheets with quantum dots and antibodies and demonstrated that these bionanoconjugates are highly sensitive and specific for the electrochemical detection of EpCAM [13]. A

Electronic supplementary material The online version of this article (https://doi.org/10.1007/s00604-020-04233-7) contains supplementary material, which is available to authorized users.

✉ Chandra Mouli Pandey
cmp.npl@gmail.com

✉ Devendra Kumar
dkumar@dce.ac.in

[1] Department of Applied Chemistry, Delhi Technological University, Delhi 110042, India

Published online: 18 April 2020

fluorescence-based biosensor using graphene quantum dots and molybdenum disulfide nanosheets have also been fabricated for rapid and sensitive detection of EpCAM [11]. Despite these achievements, still, there is a need for the fabrication of a sensitive, selective, and cost-effective biosensor that can be used for early and reliable detection of EpCAM. Nowadays, electrochemical biosensors are being widely used because of their simplicity, high sensitivity, smooth operation, accuracy, and selectivity [14]. For the fabrication of efficient electrochemical biosensor, the selection of effective transducer surfaces that bind the recognition molecule and providing faster access to the analyte is required [15]. In this context, GO has attracted tremendous interest in the fabrication of low-cost electrode materials because of its unique physical properties, such as high specific surface area, carrier mobility, electrical conductivity, flexibility, and optical transparency [16]. The oxygen-containing functional groups in GO make it strongly hydrophilic, thus facilitating the chemical functionalization that helps in the conjugation of nanoparticles and biomolecules [17–19]. Anchoring of metal oxide (ZnO, TiO_2, CuO) nanoparticles on the surface of GO with homogenous distribution exhibited improved electronic properties and served as an excellent platform for various applications [20]. Among them, TiO_2 nanoparticles have attracted considerable interest due to their superior properties, such as their large specific surface area, high uniformity, and excellent electrochemical properties. The porous nature of GO permits the penetration and adsorption of TiO_2 into the surface of GO, resulting in large surface area, better electron mobility along with more active sites for immobilization of biomolecules on the electrode surface [21, 22].

Keeping this in view, efforts have been made to synthesize rGO@TiO_2 nanocomposite using hydrothermal techniques where the GO was reduced using L-cysteine. Furthermore, rGO@TiO_2 was used as a sensing platform for the determination of EpCAM by covalently immobilizing anti-EpCAM antibodies. The response characteristics of this immunosensor pertaining to the interaction of the anti-EpCAM/rGO@TiO_2/ITO electrode with EpCAM antigen has been carried out using differential pulse voltammetry (DPV). To the best of our knowledge, the present study is the first report on the fabrication of rGO@TiO_2 nanocomposite-based transducer platform for the electrochemical determination of EpCAM cancer biomarker.

Materials and methods

All chemicals, materials, and instrumentation details are discussed in electronic supporting materials (ESM).

Synthesis of GO and TiO_2 nanoparticles

Modified Hummer's method was used for the synthesis of GO from graphite. In brief, 0.450 g of graphite powder was added to a mixture of concentrated H_2SO_4:H_3PO_4 (9:1) with constant stirring. After 10 min, 9 g of $KMnO_4$ was added to the mixture and the stirring was continued for another 12 h at 35 °C. After 12 h, the reaction was stopped and the reactants are allowed to cool at room temperature. To remove the excess of $KMnO_4$, 1.2 mL of H_2O_2 was dropped slowly and stirred for 15 min and the temperature was maintained below 20 °C. The suspension was washed with HCl (20 mL) and DI water (60 mL) and was centrifuged at 5000 rpm for 10 min. The obtained semi-solid material was vacuum dried and the solid brown powder of GO was thus obtained. The synthesized GO was dispersed in DI water (0.1 $mg{\cdot}mL^{-1}$) and sonicated for further use [23]. For the synthesis of TiO_2 nanoparticles, 15 mL of tetrabutyl titanate (TBOT) was slowly added into 1500 mL of DI water under vigorous stirring. After stirring for 3 h and aging for another 24 h, the formed gel precipitate was filtered and washed with DI water. The obtained precipitate was dried at 80 °C for 10 h and was finely powered and calcined at 500 °C for 3 h [24].

Synthesis of rGO@TiO_2 nanocomposite

For the synthesis of the rGO@TiO_2 nanocomposite, GO (10 mg) and TBOT (1.5 mmol) were added into diethylene glycol (30 mL), at constant stirring for 12 h at room temperature. The formed mixture was then added drop-wise to 180 mL of acetone, followed by the slow addition of DI water. The mixture was again stirred for 2 h that resulted in the formation of GO@TiO_2 nanocomposite that was centrifuged (15,000 rpm) and washed with water/ethanol [24]. For the reduction of the GO, the synthesized GO@TiO_2 and L-cysteine (1.5 mmol) were added into DI water (80 mL) and transferred to 100 mL autoclave for hydrothermal reaction (120 °C; 12 h). The obtained product was centrifuged (15,000 rpm), and the precipitate was collected and washed with water/ethanol (Fig. 1a) [25].

Electrophoretic deposition of rGO and rGO@TiO_2 nanocomposite

The electrophoretic deposition (EPD) of the synthesized rGO and rGO@TiO_2 nanocomposite onto hydrolyzed ITO electrode was carried out using DC power supply (Genetix, Model GX300C) using Pt as the counter electrode. For the EPD, the colloidal solution (5 mL) of rGO@TiO_2 nanocomposite (0.5 $mg{\cdot}dL^{-1}$) was diluted with 10mL ethanol which was then electrophoretically deposited onto hydrolyzed ITO electrode at 12 V for 30 s. Magnesium nitrate (10^{-4} M) was added to the above colloidal solution to obtain an adequate

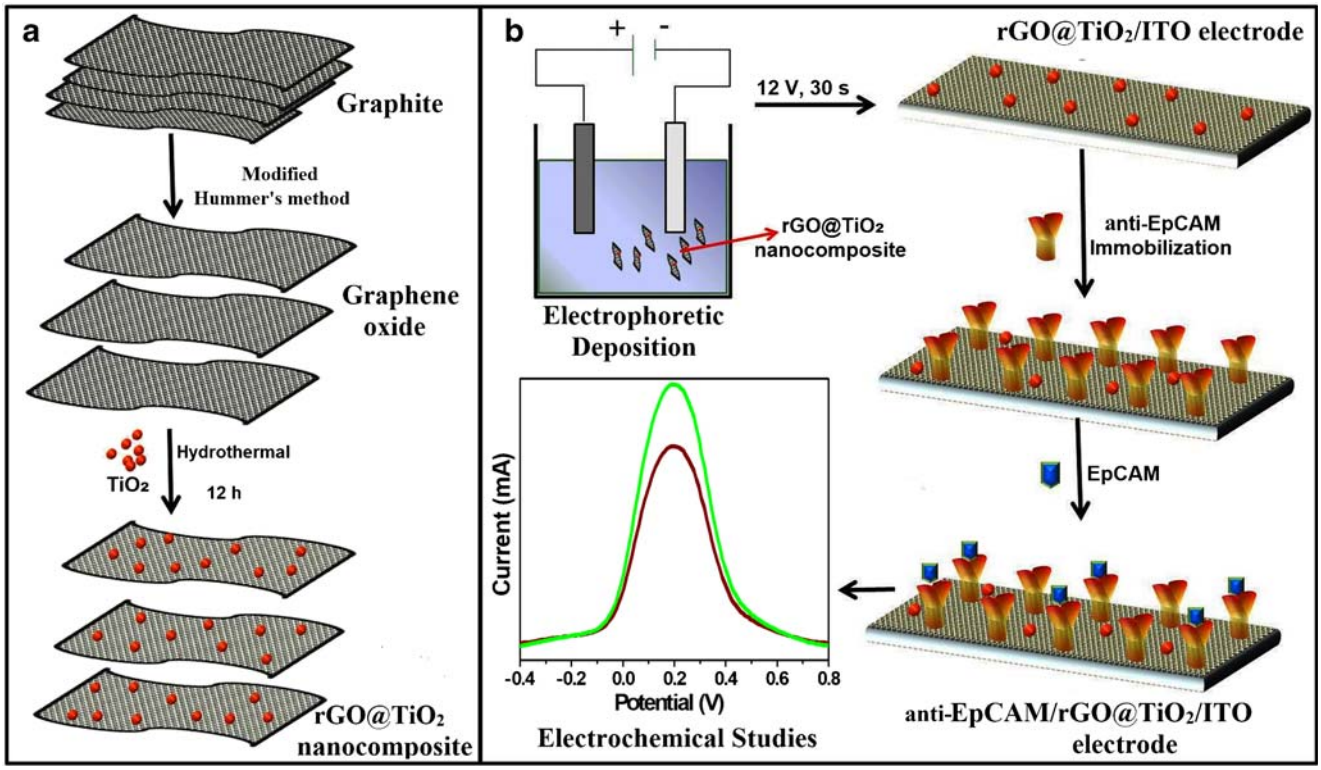

Fig. 1 Schematic illustration for the synthesis and electrophoretic deposition of rGO@TiO_2 on ITO coated glass substrate (**a**) and subsequent biosensor fabrication (**b**)

positive surface charge on the rGO@TiO_2 nanocomposite, as the Mg^{2+} ions get absorbed onto the rGO sheets. After the EPD, the electrode was taken out from the solution, washed with DI water, and dried [26].

Fabrication of rGO@TiO_2/ITO-based immunosensor

For the fabrication of immunosensor, rGO@TiO_2/ITO electrodes were treated with EDC (2 mM; 10 μL) and NHS (5 mM; 10 μL) for 1 h at room temperature (27 °C), to activate the –COOH functional groups. Furthermore, the modified electrodes were incubated with 20 μL (50 μg mL^{-1}) of monoclonal antibodies (anti-EpCAM) in PBS containing Tween-20 (0.05%). To avoid non-specific antigen binding, the anti-EpCAM/rGO@TiO_2/ITO electrodes were treated with BSA (1%) for 2 h to block the exposed binding sites of the electrode, followed by washing with PBS (3 times). The schematic for the fabrication of the immunosensor has been shown in Fig. 1b.

Choice of materials

A novel electrochemical biosensor based on rGO@TiO_2 nanocomposite has been proposed for the determination of EpCAM cancer biomarker. Nanocomposites based on GO@TiO_2 have been previously reported, but the application was limited mainly to lithium-ion batteries, photocatalysis, or energy-related fields [27]. Very few reports for utilizing GO@TiO_2 nanocomposite in sensing applications are available still, more research is needed to explore this highly desirable nanocomposite material in the biosensing field. Furthermore, the extremely large surface area and remarkable conducting properties of GO along with a high isoelectric point of TiO_2 may provide a new opportunity to utilize this rGO@TiO_2 nanocomposite for designing efficient biosensors. The modified electrode (rGO@TiO_2/ITO electrodes) can effectively enhance the electrochemical performance along with more active sites for the immobilization of biomolecules.

Results and discussion

The TEM images of GO sheet display a crumbled and restacked morphology (Fig. 2a) with a large surface area (few micrometers in the diameter). This large surface area provides an advantage for the growth of TiO_2 nanoparticles on the GO surface. Figure 2b shows the TEM micrograph of rGO@TiO_2 nanocomposite, where spherically polycrystalline TiO_2 nanoparticles (30–40 nm) are evenly distributed on the GO sheet. So, it can be revealed that GO acts as an excellent platform for entrapping TiO_2 nanoparticles. The formation of GO, rGO, and rGO@TiO_2 nanocomposite has also been confirmed

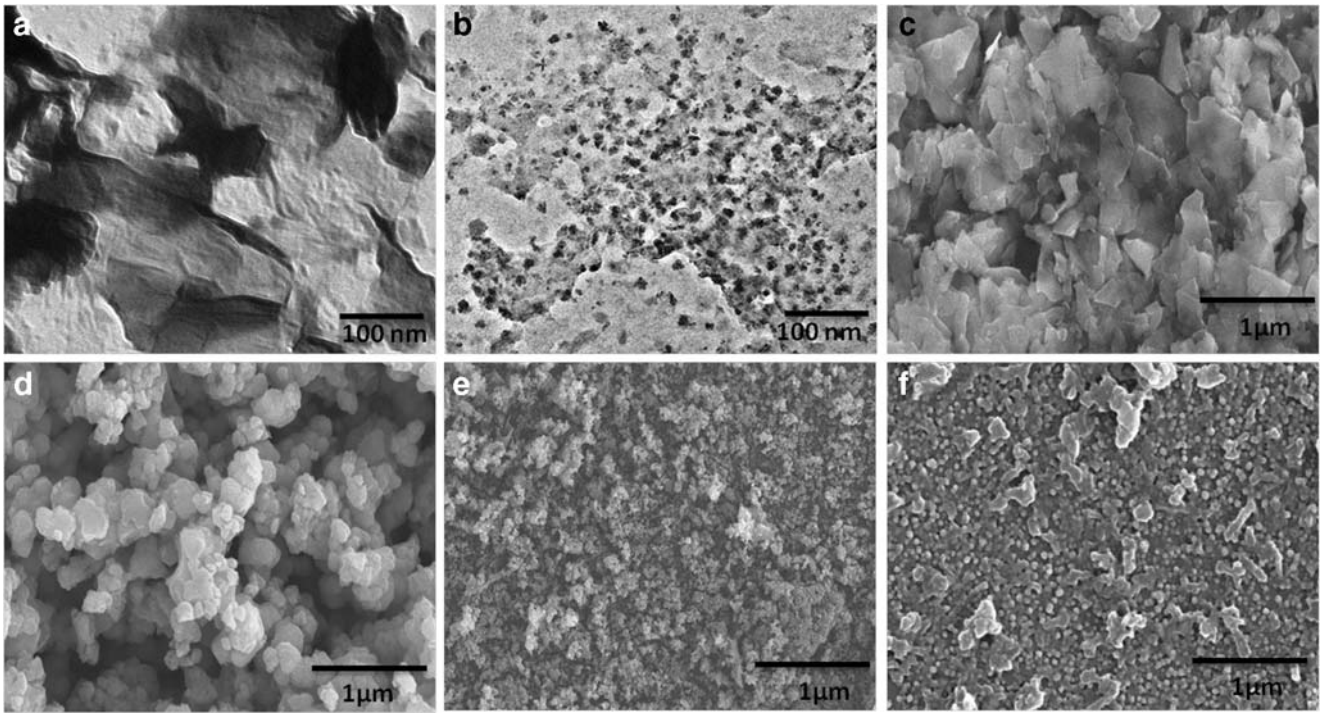

Fig. 2 Transmission electron microscopic image of GO (**a**) and rGO@TiO_2 nanocomposite (**b**). Scanning electron microscopic images of rGO/ITO electrode (**c**), TiO_2/ITO electrode (**d**), rGO@TiO_2/ITO electrode (**e**), and anti-EpCAM/rGO@TiO_2/ITO electrode (**f**)

using X-ray diffraction pattern (Fig. S1A and B), UV-vis spectrum (Fig. S2A and B), TGA (Fig. S3A), and FTIR (Fig. S3B and C) (respective text and figures are given in the Electronic Supporting Material).

The SEM image of the rGO/ITO electrode (Fig. 2c) shows a large sheet-like structure with thin curtains like morphology, which is due to the delaminating of graphite during the oxidation process. Figure 2d shows the SEM micrograph for the TiO_2 nanoparticles, having a spherical shape with good dispersion and less agglomeration. Furthermore, the surface morphology of GO changes after modification with TiO_2 and shows the surface of rGO covered with spherical TiO_2 nanoparticles (Fig. 2e). After the immobilization of anti-EpCAM onto the surface of rGO@TiO_2/ITO electrode, the granular morphology becomes globular due to covalent attachment of antibodies (Fig. 2f).

Electrochemical characterization

Electrochemical studies of the rGO/ITO electrode, rGO@TiO_2/ITO electrode, and anti-EpCAM/rGO@TiO_2/ITO bioelectrode have been performed in PBS containing 5 mM of $[Fe(CN)_6]^{3-/4-}$ using electrochemical impedance spectroscopy (EIS) in the frequency range 0.01–10^5 Hz. The electrochemical impedance spectra (Nyquist plots) mainly include a semicircle portion at higher frequencies, followed by a linear part at lower frequencies corresponding to electron transfer–limited process and a diffusion-limited electron transfer process, respectively [28]. The semicircle diameter gives the value of charge transfer resistance (R_{ct}) and can be derived numerically by fitting an equivalent circuit based on the modified Randles and Ershler model [29]. The characteristic Nyquist plots for the fabricated electrodes are shown in Fig. 3a along with the fitted Randles equivalent circuit (Fig. 3a; inset). The circuit consists of an electron transfer resistance (R_{ct}), constant phase element (C_{PE}), solution resistance (R_s), and Warburg impedance (W) [30]. The EIS curve of rGO/ITO electrode shows a R_{ct} value of 1.35 kΩ (curve (ii)), which is attributed to good conductivity of GO that facilitates fast transfer of electrons. However, for the rGO@TiO_2/ITO electrode (curve (i)), there is a decrease in the R_{ct} value (1.12 kΩ). This decrease in R_{ct} can be assigned to the synergistic effects of GO sheets and TiO_2 that enhance the electrochemical performance of rGO@TiO_2/ITO electrode. Furthermore, after immobilization of anti-EpCAM onto rGO@TiO_2/ITO electrode (curve (iii)) and blocking of exposed electrode site using BSA, there is an increase in the R_{ct} value (1.68 kΩ). This increase in R_{ct} can be due to the non-conducting nature of antibody that hinders the charge transfer pathway. When the target antigen was incubated to anti-EpCAM/rGO@TiO_2/ITO electrode, an antibody-antigen complex has been formed that creates a barrier for the electrochemical transduction process, thereby hindering the access of the redox probe to the electrode surface and thus increasing the R_{ct} (2.53 kΩ) [31]. In the EIS spectra, the reaction occurring at the electrode is governed

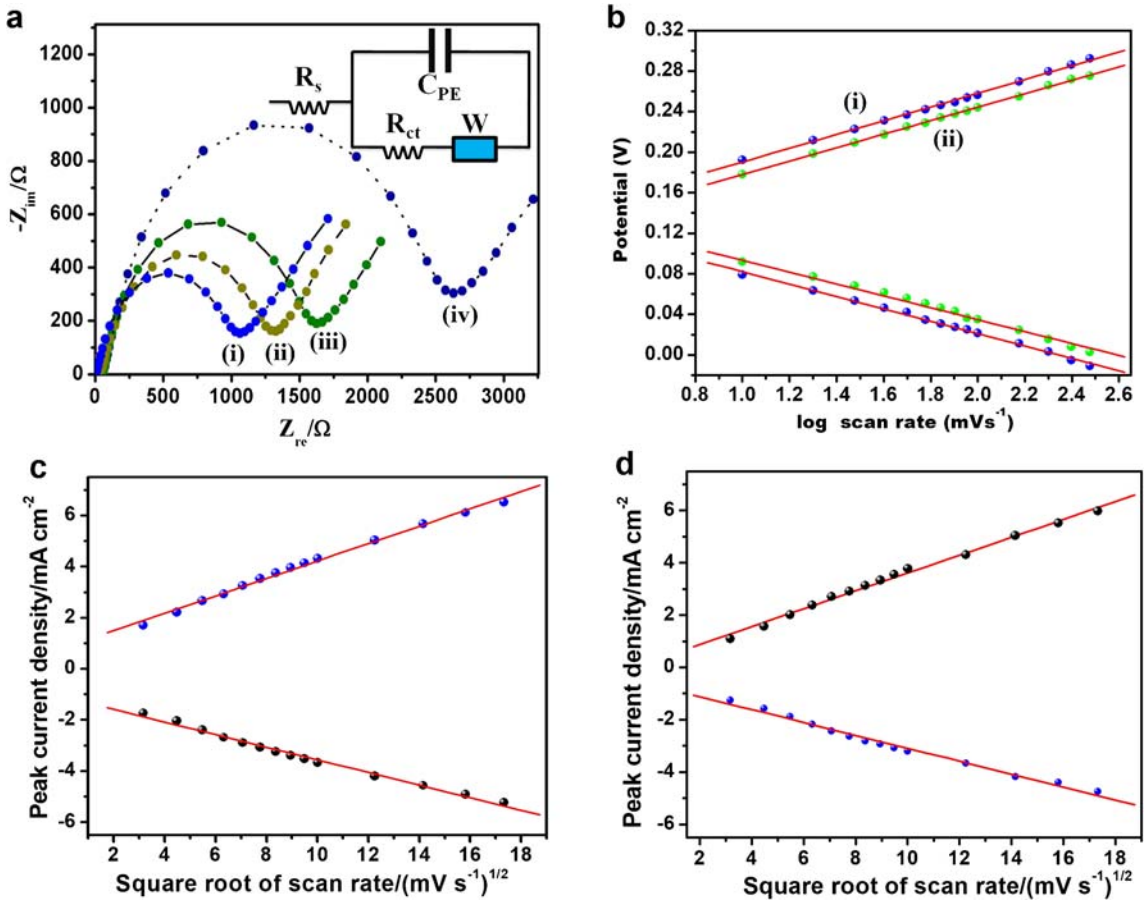

Fig. 3 (**a**) Nyquist diagram for the Faradic impedance for (i) rGO@TiO_2/ITO electrode, (ii) rGO/ITO electrode, (iii) anti-EpCAM/rGO@TiO_2/ITO electrode, and (iv) EpCAM immobilized on anti-EpCAM/rGO@TiO_2/ITO electrode measured in PBS solution (pH 7.4) containing 5 mM $[Fe(CN)_6]^{3-/4-}$, in the frequency range from 10^5 to 10^{-2} Hz. (**b**) The plots of potential with log of scan rate for (i) rGO@TiO_2/ITO electrode and (ii) rGO/ITO electrode. The plot for I_{pa}, I_{pc}, vs. square root of scan rate (10–300 mV) for the rGO@TiO_2/ITO electrode and (**c**) rGO/ITO electrode (**d**) in PBS solution (pH 7.4) containing 5 mM $[Fe(CN)_6]^{3-/4-}$

by the electron–transfer kinetics. Thus, the exchange current per geometric unit area ($i_o = nRT/R_{ct}F$) for the rGO/ITO electrode and rGO@TiO_2/ITO electrode is found to be 7.60×10^{-5} A·cm^{-2} and 9.32×10^{-5} A·cm^{-2}, respectively. The apparent electron transfer rate constant (k_{app}) for the modified electrodes is also calculated using the equation: $k_{app} = RT/n^2F^2AR_{ct}C$; where F is the Faraday constant, n denotes the number of electrons transferred, R is the gas constant, T is the temperature in Kelvin, A is the area of the electrode, and C is the concentration of the $[Fe(CN)_6]^{3-/4-}$. The values of k_{app} are found to be 1.57×10^{-7} cm·s^{-1} and 1.93×10^{-7} cm·s^{-1} for the rGO/ITO electrode and rGO@TiO_2/ITO electrode, respectively. It has been observed that the peak current density of cyclic voltammetry (CV) is proportional to the square root of the scan rate, revealing the linear dependence of peak currents to the scan rate. This indicates that the electron transfer from rGO/ITO and rGO@TiO_2/ITO electrode is a surface-controlled process [32]. When the scan rate (υ) was increased from 10 to 300 mV·s^{-1}, the oxidation peak drifts to a more positive value and the reduction peak to more negative values. This shows that both the peak potentials (E_p and E_c) are linearly dependent on the log υ (Fig. 3b) and yields two straight lines (Eqs. 1, 2, 3, and 4) with anodic and cathodic slopes of $2.303RT/(1-\alpha)nF$ and $-2.303RT/\alpha nF$, respectively.

$$E_p(V)[rGO@TiO_2/ITO] = 0.124(V) + 0.067(V) \times Log[scanrate(mV/s)]; R^2 = 0.998 \quad (1)$$

$$E_c(V)\ [rGO@TiO_2/ITO] = 0.143(V) - 0.060\ (V) \times Log\ [scan\ rate\ (mV/s)]; R^2 = 0.994 \quad (2)$$

$$E_p(V)\ [rGO/ITO] = 0.115\ (V) + 0.067\ (V) \times \mathrm{Log}\ [\text{scan rate}\ (mV/s)];\ R^2 = 0.996 \quad (3)$$

$$E_c(V)\ [rGO/ITO] = 0.151(V) - 0.058\ (V) \times \mathrm{Log}\ [\text{scan rate}\ (mV/s)];\ R^2 = 0.987 \quad (4)$$

Based on the plot and the above equation, the values of α are estimated to be 0.59 for rGO/ITO electrode and 0.61 for rGO@TiO_2/ITO electrode. The effective surface area (A) was calculated using the linear slope of the anodic and cathodic peak currents density (I_{pa} and I_{pc}) on the square root of scan rate (Fig. 3c, d; Eqs. 5, 6, 7, and 8), and the Randle Sevick equation: $Ip = (2.69 \times 10^5)n^{3/2}ACD^{1/2}\ \upsilon^{1/2}$. Where Ip is the peak current, C is the molar concentration of $[Fe(CN)_6]^{3-/4-}$ ($mol \cdot cm^{-3}$), n is the electrons per molecule oxidized or reduced, D is the diffusion coefficient, and υ is the scan rate. The effective surface area (A) of the rGO@TiO_2/ITO electrode ($D = 1.31 \times 10^{-5}\ cm^2 \cdot s^{-1}$) is found to be 0.075 cm^2. The A calculated for rGO/ITO electrode and ITO electrode is found to be 0.086 cm^2 ($D = 0.89 \times 10^{-5}\ cm^2 \cdot s^{-1}$) and 0.10 cm^2 ($D = 0.53 \times 10^{-5}\ cm^2 \cdot s^{-1}$), respectively.

$$I_{pa}\ (\mu A)\ [rGO@TiO_2/ITO] = 631.4\ \mu A + 367.0\ \mu A\ (s \cdot mV^{-1}) \times \text{scan rate}\ (mV \cdot s^{-1});\ R^2 = 0.999 \quad (5)$$

$$I_{pc}(\mu A)[rGO@TiO_2/ITO] = -110.2\mu A - 246.8\mu A(s \cdot mV^{-1}) \times \text{scanrate}(mV \cdot s^{-1});\ R^2 = 0.996 \quad (6)$$

$$I_{pa}(\mu A)[rGO/ITO] = 63.1\mu A - 345.1\mu A(s \cdot mV^{-1}) \times \text{scanrate}(mV \cdot s^{-1});\ R^2 = 0.998 \quad (7)$$

$$I_{pc}(\mu A)[rGO/ITO] = -626.8\mu A - -241.7\mu A(s \cdot mV^{-1}) \times \text{scanrate}(mV \cdot s^{-1});\ R^2 = 0.987 \quad (8)$$

Optimization of biosensing parameters

The concentration of anti-EpCAM required for binding onto the surface of rGO@TiO_2/ITO electrode using EDC-NHS chemistry was also optimized using DPV and is found to be 50 $\mu g \cdot mL^{-1}$ (Fig. S4A). The maximum binding time of EpCAM (1 $ng \cdot mL^{-1}$) antigen with the anti-EpCAM/rGO@TiO_2/ITO electrode has been achieved in 10 min (Fig. S4B).

Electrochemical biosensing studies

DPV studies were carried out for ITO electrode, rGO/ITO electrode, rGO@TiO_2/ITO electrode, and anti-EpCAM/rGO@TiO_2/ITO electrode to study the effect of electrode modification at a various step (the respective data and figures are given in the Electronic Supporting Materials (Fig. S5)). To examine the efficacy of the biosensor, electrochemical studies of the anti-EpCAM/rGO@TiO_2/ITO electrode were carried out as a function of EpCAM concentration (0.01–60 $ng \cdot mL^{-1}$) in PBS containing 5 mM $[Fe(CN)_6]^{3-/4-}$ using DPV. A continuous decrease in the anodic peak current has been observed when the anti-EpCAM/rGO@TiO_2/ITO electrode was treated with an increasing concentration of EpCAM (Fig. 4a). This decrease in the response current is due to the interaction of EpCAM with anti-EpCAM at the transducer surface that results in the formation of an insulating layer (antigen-antibody complex) on the electrode surface that retards the electron transfer from the bulk solution to the electrode. Figure 4b shows the calibration plot for the change in the magnitude of the peak current of anti-EpCAM/rGO@TiO_2/ITO electrode as a function of EpCAM concentration (0.01–60 $ng \cdot mL^{-1}$) and follows Eq. (9):

$$I_p = 0.025(\mu A) - 0.814(\mu A \cdot mL \cdot ng^{-1}) \times \text{EpCAM concentration}(ng \cdot mL^{-1}) \quad (9)$$

The sensitivity (slope/surface area) calculated for anti-EpCAM/rGO@TiO_2/ITO electrode is 3.24 $\mu A \cdot mL \cdot ng^{-1} \cdot cm^{-2}$ with a correlation coefficient of 0.997. The limit of detection (LOD) calculated (3σ/sensitivity), for the fabricated biosensor is 0.0065 $ng \cdot mL^{-1}$ or 240 fM ($S/N = 3$), where σ is the standard deviation of the blank electrode. For all the sensing experiments, anti-EpCAM/rGO@TiO_2/ITO electrode with PBS solution was taken as a control signal, and the imprecision of the data (Fig. 4b) is found to be < 3%. The biosensing performance of the fabricated anti-EpCAM/rGO@TiO_2/ITO electrode has been compared with other methods for EpCAM detection (Table 1). The fabricated biosensor achieved a LOD of 0.0065 $ng \cdot mL^{-1}$ that is comparable with the other reported biosensors [11–13, 33]. The enhanced electrochemical performance of anti-EpCAM/rGO@TiO_2/ITO electrode can be attributed to the good conductivity of rGO@TiO_2 that improves the local topographic interactions with the anti-EpCAM [34]. The fabricated biosensor was also compared with other reported TiO_2-based biosensors for cancer biomarker determination, and it has been observed that the proposed method shows significant results (Table S1). To determine the affinity of EpCAM toward anti-EpCAM/

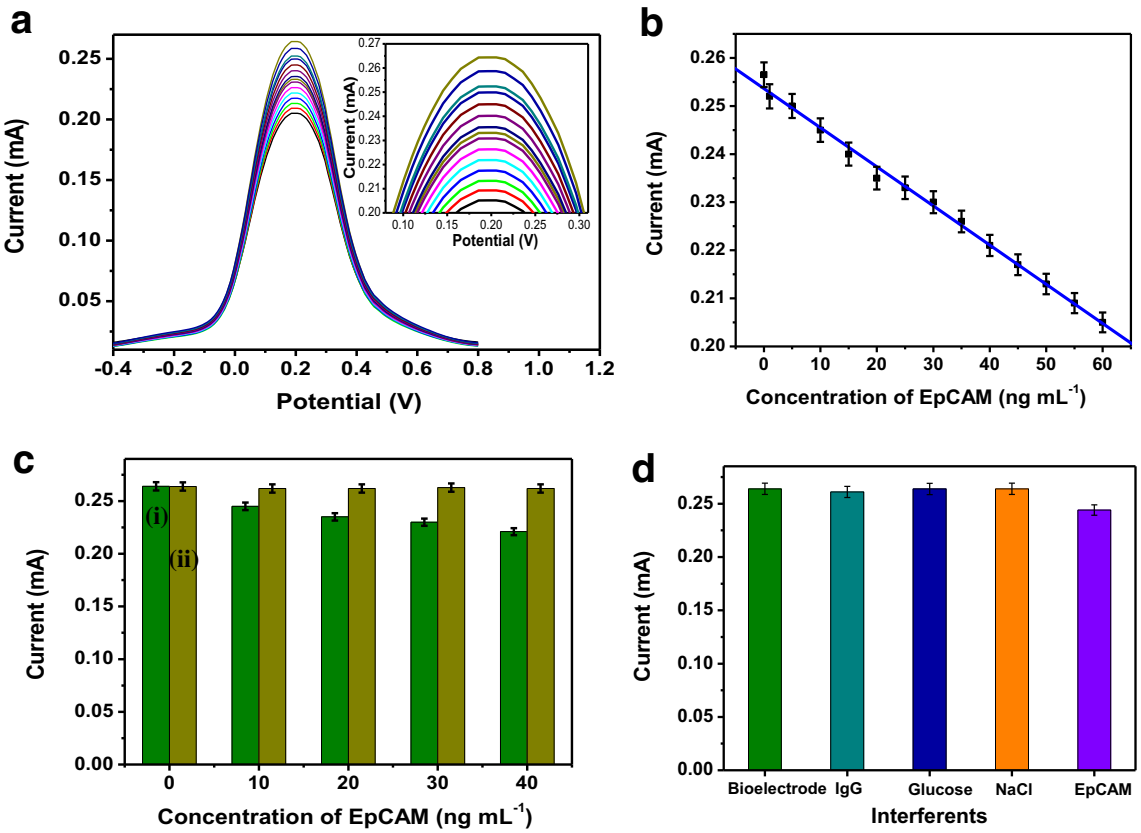

Fig. 4 Electrochemical response of the anti-EpCAM/rGO@TiO_2/ITO electrode (**a**) as a function of EpCAM concentration (from top to bottom, 0 to 60 ng·mL^{-1}) using DPV; inset is the magnified view of oxidation peak current. (**b**) Calibration plot between the magnitudes of current recorded and EpCAM concentration (0.01–60 ng·mL^{-1}). Error bars represent the standard deviations of repeated determinations (n = 3). (**c**) Control experiment showing the DPV response of (i) anti-EpCAM/rGO@TiO_2/ITO electrode and (ii) rGO@TiO_2/ITO electrode against EpCAM. (**d**) Specificity testing of anti-EpCAM/rGO@TiO_2/ITO-based biosensor with glucose and IgG proteins as control groups. The measurements were conducted by scanning the potential from − 0.4 to 0.8 V with an amplitude of 50 mV in PBS solution (pH 7.4) containing 5 mM $[Fe(CN)_6]^{3-/4-}$. Error bars: SD, n = 3

rGO@TiO_2/ITO electrode, the association constant (K_a) has been calculated using the Hanes–Wolf plot [35] and the higher is the value of K_a, the stronger is the affinity of EpCAM toward anti-EpCAM/rGO@TiO_2/ITO electrode. The K_a estimated (plot between substrate concentrations versus substrate concentration/current) is found to be 4.86×10^{-15} M^{-1}.

Table 1 Biosensing characteristics of anti-EpCAM/rGO@TiO_2/ITO electrode along with those reported in the literature

S. no.	Immobilization matrix	Biomolecule	Detection technique	Linear detection range	Detection limit	Labeling	Sensitivity	Ref.
1.	GQDs-MoS_2	Aptamer	Fluorescence	3–54 nM	450 pM	Yes	–	[11]
2.	LC-SPDP/Au	Antibody	CV and Fluorescence	1×10^5–1×10^8 cells mL^{-1}	1×10^5 cells mL^{-1}	Yes	–	[12]
3.	Rubpy core-shell Silica	Antibody	Fluorescence and FCM	–	–	Yes	–	[33]
4.	GRs-QDs	Antibody	ASV	100 fg·mL^{-1} - 7.5 μg·mL^{-1}	100 fg·mL^{-1}	Yes	–	[13]
5.	AgNPs-PVA	Antibody	EM	2–2000 pg·mL^{-1}	0.8 pg·mL^{-1}	No	–	[36]
6.	MCH/Hp1/AuE	Aptamer	SWV	0.1–20 ng·mL^{-1}	20 pg·mL^{-1}	Yes	–	[37]
7.	rGO-TiO_2/ITO	Antibody	DPV	0.01–60 ng·mL^{-1}	6.5 pg·mL^{-1} or 240 fM	No	3.24 μA·mL·ng^{-1} ·cm^{-2}	Present work

GQDs, graphene quantum dots; *MoS_2*, molybdenum disulphide; *LC-SPDP*, succinimidyl 6-(3-[2-pyridyldithio]-propionamido) hexanoate; *Au*, gold; *Rubpy*, tris(bipyridine)ruthenium(II)chloride; *GRs*, graphene oxide nanosheets; *QDs*, quantum dots; *AgNPs-PVA*, silver nanoparticles covered with polyvinyl alcohol; *MCH/Hp1/AuE*, 6-mercapto-1-hexanol/hairpin probe 1/gold electrode; *FCM*, flow cytometer; *ASV*, anodic stripping voltammetry; *EM*, electrochemical microfluidic; *SWV*, square wave voltammetry

Electrochemical studies were also conducted to evaluate the current response of bare rGO@TiO_2/ITO electrode toward different concentrations of EpCAM (Fig. 4c). The obtained results indicate that there is no significant change in the peak current, revealing no false signal is generated, and the electrochemical response is completely due to the interaction between EpCAM and anti-EpCAM/rGO@TiO_2/ITO electrode.

Stability and regenerability of the biosensor

The stability and reusability of the biosensor have also been tested. It was observed that after 35 days, the current response of the immunosensor remains 93.7% of the initial value (Fig. S6A). Furthermore, the bioelectrode can be regenerated and reused, for at least 5 times with a relative standard deviation of 6.6% (Fig. S6B).

Specificity and serum sample analysis

The specificity of the fabricated immunosensor for EpCAM detection was carried out by incubating the anti-EpCAM/rGO@TiO_2/ITO electrode with glucose, immunoglobulin G (IgG), sodium chloride (NaCl), and EpCAM with the same concentration (15 ng·mL^{-1}). These analytes are typical interfering species that exist in human plasma. The bar diagram (Fig. 4d) clearly shows that no false signal has been generated when the electrode was treated with glucose, IgG, and NaCl showing good specificity of the biosensor for EpCAM detection.

To validate the performance of the fabricated biosensor, the electrochemical response studies of the anti-EpCAM/rGO@TiO_2/ITO electrode with spiked human serum samples at 5, 10, 15, and 20 ng·mL^{-1} were performed (Table S2). The spiked serum samples have been prepared by adding 20 μL of EpCAM into 100 μL of serum. The observed results exhibited acceptable recoveries (98–101%) with relative standard deviation of 1.8–4.7% (n = 3) of EpCAM in serum samples. This suggests that the fabricated immunosensor can be an alternative technique for the determination of EpCAM in human serum.

Conclusion

A highly sensitive electrochemical biosensor has been fabricated for the determination of cancer biomarker using rGO@TiO_2 nanocomposite. The environment-friendly route was used for the synthesis of the nanocomposite, which shows excellent electrochemical properties, selectivity and performs as an appropriate sensing layer. The GO-based substrate provides an excellent platform for the growth of TiO_2 nanoparticles and with covalent conjugation of anti-EpCAM, it shows a much lower detection limit. This fabricated biosensor was validated with spiked serum samples and it shows a promising result for the efficient detection of cancer biomarkers in the serum sample. It is believed that the fabricated platform has the potential to be used for the monitoring of other cancer biomarkers, which would be transformative in the diagnosis of cancer. Besides this, more efforts are needed to develop straight forward methods for the determination of the EpCAM profile for circulating tumor cells.

Acknowledgements C.M. Pandey acknowledges the Department of Science and Technology (DST), New Delhi, India, for DST-INSPIRE Faculty award (Grant No. DST/INSPIRE/04/2015/000932).

Compliance with ethical standards

Conflict of interest The authors declare that they have no conflict of interest.

References

1. Gorges TM, Tinhofer I, Drosch M, Röse L, Zollner TM, Krahn T, von Ahsen O (2012) Circulating tumour cells escape from EpCAM-based detection due to epithelial-to-mesenchymal transition. BMC Cancer 12:178
2. Gostner JM, Fong D, Wrulich OA, Lehne F, Zitt M, Hermann M, Krobitsch S, Martowicz A, Gastl G, Spizzo G (2011) Effects of EpCAM overexpression on human breast cancer cell lines. BMC Cancer 11:45
3. Treerattrakoon K, Chanthima W, Apiwat C, Dharakul T, Bamrungsap S (2017) Oriented conjugation of antibodies against the epithelial cell adhesion molecule on fluorescently doped silica nanoparticles for flow-cytometric determination and in vivo imaging of EpCAM, a biomarker for colorectal cancer. Microchim Acta 184:1941–1950
4. Patriarca C, Macchi RM, Marschner AK, Mellstedt H (2012) Epithelial cell adhesion molecule expression (CD326) in cancer: a short review. Cancer Treat Rev 38:68–75
5. Yoon HJ, Kozminsky M, Nagrath S (2014) Emerging role of nanomaterials in circulating tumor cell isolation and analysis. ACS Nano 8:1995–2017
6. Ntouroupi T, Ashraf S, McGregor S, Turney B, Seppo A, Kim Y, Wang X, Kilpatrick M, Tsipouras P, Tafas T (2008) Detection of circulating tumour cells in peripheral blood with an automated scanning fluorescence microscope. Br J Cancer 99:789–795
7. Zhao S, Yang H, Zhang M, Zhang D, Liu Y, Liu Y, Song Y, Zhang X, Li H, Ma W (2013) Circulating tumor cells (CTCs) detected by triple-marker EpCAM, CK19, and hMAM RT-PCR and their relation to clinical outcome in metastatic breast cancer patients. Cell Biochem Biophys 65:263–273
8. Lambrechts AC, Bosma AJ, Klaver S, Top B, Perebolte L, Van't Veer L, Rodenhuis S (1999) Comparison of immunocytochemistry, reverse transcriptase polymerase chain reaction, and nucleic acid sequence–based amplification for the detection of circulating breast cancer cells. Breast Cancer Res Treat 56:219–231
9. Shen H, Yang J, Chen Z, Chen X, Wang L, Hu J, Ji F, Xie G, Feng W (2016) A novel label-free and reusable electrochemical cytosensor for highly sensitive detection and specific collection of CTCs. Biosens Bioelectron 81:495–502
10. Li Z, Wang Y, Wang J, Tang Z, Pounds JG, Lin Y (2010) Rapid and sensitive detection of protein biomarker using a portable

fluorescence biosensor based on quantum dots and a lateral flow test strip. Anal Chem 82:7008–7014
11. Shi J, Lyu J, Tian F, Yang M (2017) A fluorescence turn-on biosensor based on graphene quantum dots (GQDs) and molybdenum disulfide (MoS2) nanosheets for epithelial cell adhesion molecule (EpCAM) detection. Biosens Bioelectron 93:182–188
12. Arya SK, Wang KY, Wong CC, Rahman ARA (2013) Anti-EpCAM modified LC-SPDP monolayer on gold microelectrode based electrochemical biosensor for MCF-7 cells detection. Biosens Bioelectron 41:446–451
13. Shiddiky MJA, Rauf S, Kithva PH, Trau M (2012) Graphene/quantum dot bionanoconjugates as signal amplifiers in stripping voltammetric detection of EpCAM biomarkers. Biosens Bioelectron 35:251–257
14. Chikkaveeraiah BV, Bhirde AA, Morgan NY, Eden HS, Chen X (2012) Electrochemical immunosensors for detection of cancer protein biomarkers. ACS Nano 6:6546–6561
15. Soni A, Pandey CM, Solanki S, Kotnala RK, Sumana G (2018) Electrochemical genosensor based on template assisted synthesized polyaniline nanotubes for chronic myelogenous leukemia detection. Talanta 187:379–389
16. Zhu Y, Murali S, Cai W, Li X, Suk JW, Potts JR, Ruoff RS (2010) Graphene and graphene oxide: synthesis, properties, and applications. Adv Mater 22:3906–3924
17. Hussein KH, Abdelhamid HN, Zou X, Woo H-M (2019) Ultrasonicated graphene oxide enhances bone and skin wound regeneration. Mater Sci Eng C 94:484–492
18. Hallaj R, Haghighi N (2017) Photoelectrochemical amperometric sensing of cyanide using a glassy carbon electrode modified with graphene oxide and titanium dioxide nanoparticles. Microchim Acta 184:3581–3590
19. Sanghavi BJ, Wolfbeis OS, Hirsch T, Swami NS (2015) Nanomaterial-based electrochemical sensing of neurological drugs and neurotransmitters. Microchim Acta 182:1–41
20. Ashour RM, Abdelhamid HN, Abdel-Magied AF, Abdel-Khalek AA, Ali MM, Uheida A, Muhammed M, Zou X, Dutta J (2017) Rare earth ions adsorption onto graphene oxide nanosheets. Solvent Extr Ion Exch 35:91–103
21. Jang HD, Kim SK, Chang H, Roh K-M, Choi J-W, Huang J (2012) A glucose biosensor based on TiO_2–graphene composite. Biosens Bioelectron 38:184–188
22. Josephine DSR, Babu KJ, Gnana Kumar G, Sethuraman K (2017) Titanium dioxide anchored graphene oxide nanosheets for highly selective voltammetric sensing of dopamine. Microchim Acta 184: 781–790
23. Shahriary L, Athawale AA (2014) Graphene oxide synthesized by using modified hummers approach. Int J Renew Energy Environ Eng 2:58–63
24. Perera SD, Mariano RG, Vu K, Nour N, Seitz O, Chabal Y, Balkus KJ (2012) Hydrothermal synthesis of graphene-TiO_2 nanotube composites with enhanced photocatalytic activity. ACS Catal 2: 949–956
25. Pandey CM, Tiwari I, Singh VN, Sood K, Sumana G, Malhotra BD (2017) Highly sensitive electrochemical immunosensor based on graphene-wrapped copper oxide-cysteine hierarchical structure for detection of pathogenic bacteria. Sens Actuators B Chem 238: 1060–1069
26. Srivastava S, Kumar V, Ali MA, Solanki PR, Srivastava A, Sumana G, Saxena PS, Joshi AG, Malhotra BD (2013) Electrophoretically deposited reduced graphene oxide platform for food toxin detection. Nanoscale 5:3043–3051
27. Fan W, Lai Q, Zhang Q, Wang Y (2011) Nanocomposites of TiO_2 and reduced graphene oxide as efficient photocatalysts for hydrogen evolution. J Phys Chem C 115:10694–10701
28. Randviir EP, Banks CE (2013) Electrochemical impedance spectroscopy: an overview of bioanalytical applications. Anal Methods 5:1098–1115
29. Randles JEB (1947) Kinetics of rapid electrode reactions. Discuss Faraday Soc 1:11–19
30. Jorcin J-B, Orazem ME, Pébère N, Tribollet B (2006) CPE analysis by local electrochemical impedance spectroscopy. Electrochim Acta 51:1473–1479
31. Xie Y, Chen A, Du D, Lin Y (2011) Graphene-based immunosensor for electrochemical quantification of phosphorylated p53 (S15). Anal Chim Acta 699:44–48
32. Pandey CM, Sumana G, Tiwari I (2014) Copper oxide assisted cysteine hierarchical structures for immunosensor application. Appl Phys Lett 105:103706
33. Tao L, Zhang K, Sun Y, Jin B, Zhang Z, Yang K (2012) Anti-epithelial cell adhesion molecule monoclonal antibody conjugated fluorescent nanoparticle biosensor for sensitive detection of colon cancer cells. Biosens Bioelectron 35:186–192
34. Dowaidar M, Abdelhamid HN, Hällbrink M, Zou X, Langel Ü (2017) Graphene oxide nanosheets in complex with cell penetrating peptides for oligonucleotides delivery. BBA-Gen Subjects 1861: 2334–2341
35. Augustine S, Joshi AG, Yadav BK, Mehta A, Kumar P, Renugopalakrishanan V, Malhotra BD (2018) An emerging nanostructured molybdenum trioxide-based biocompatible sensor platform for breast cancer biomarker detection. MRS Commun 8:668–679
36. Bravo K, Ortega FG, Messina GA, Sanz MI, Fernández-Baldo MA, Raba J (2017) Integrated bio-affinity nano-platform into a microfluidic immunosensor based on monoclonal bispecific trifunctional antibodies for the electrochemical determination of epithelial cancer biomarker. Clin Chim Acta 464:64–71
37. Chen Q, Hu W, Shang B, Wei J, Chen L, Guo X, Ran F, Chen W, Ding X, Xu Y (2018) Ultrasensitive amperometric aptasensor for the epithelial cell adhesion molecule by using target-driven toehold-mediated DNA recycling amplification. Microchim Acta 185:202

Publisher's note Springer Nature remains neutral with regard to jurisdictional claims in published maps and institutional affiliations.